Shock and Vibration 20 (2013) 97–108
DOI 10.3233/SAV-2012-0730
IOS Press

Transfer matrix method to vibration analysis of rotors with coupler offsets

Chao-Yang Tsai[a] and Shyh-Chin Huang[b,*]
[a]*Department of Mechanical Engineering, Army Academy ROC, Taoyuan, Taiwan*
[b]*Department of Mechanical Engineering, Ming Chi University of Technology, Taipei, Taiwan*

Received 17 May 2012
Revised 4 June 2012

Abstract. In this paper a general transfer matrix method (TMM) for rotors containing global and local coupler offset was derived. Rotor response due to imbalances and offsets are then studied via the developed method. The studies showed both global and local offsets played as an external excitation that is a combined effect of all the elements behind the offset. Differences between global offset and local offset were compared and the results showed both types basically retain the same mode patterns but different jumps at the offset. The global offset, yet, imposed more significant dynamic effects since all the offsets accumulate thereafter. The whirling orbits in front and behind the offset were illustrated as well. The results, as expected, showed global offset appeared much larger radii especially after offset. The rotor's whirling orientation reversed, as rotation fell within a certain range and this feature was not changed by offsets. The TMM proposed by this study can be well applied to multiple global and local offsets.

Keywords: Transfer matrix method, misalignment, unbalance, shaft offset

1. Introduction

Rotors have been extensively used in mechanical engineering. The dynamic behaviour of rotors has hence gained interests for over a century. With the high speed demand of today's machinery, the studies of rotors become more important than ever. Approaches to dynamic analysis of rotor systems can be divided into two main branches. One is the widely used finite element method (FEM) [1–3], and the other is the relatively more traditional one, the transfer matrix method (TMM) [4] The main advantage of TMM is its fixed matrix dimensions despite the complexity of rotor composition. Its disadvantage is yet the necessity of more matrices multiplications and a sophisticated root finding algorithm.

Among the existing TMM literature, Prohl [5], one of the pioneers, derived it for critical speed analysis of rotor systems. Lund and Orcutt [6] developed shaft's transfer matrix in a continuous fashion but neglected both the rotary inertia and the gyroscopic effect. Lund [7] considered the internal hysteretic shaft damping and the destabilizing aerodynamic forces to calculate the damped natural frequencies of a general flexible rotor supported in fluid-film journal bearing. Chao and Huang [8] introduced a modify transfer matrix in which the Euler beam and rigid disk were the fundamental element and improved the accuracy of natural frequencies and shapes. Many researchers [9–11] continuously improved TMM, such as developing an oil-film bearing matrix, adding rotary inertia and the disk's gyroscopic effects. Yet, to the authors' knowledge, none of them derived the commonly seen cases of misaligned/offset coupler in TMM. Until lately, the present authors derived the offset coupler transfer matrix and extended it to multiple offsets rotors [12]. In the existing literature, as the coupler offset was referred, there

*Corresponding author: Shyh-Chin Huang, Department of Mechanical Engineering, Ming Chi University of Technology, 84 Gongzhuan Rd., Taishan, New Taipei City 24301, Taiwan. Tel.: +886 229 089 899 ext.4563; Fax: +886 229 041 914; E-mail: schuang@mail.ntust.edu.tw.

ISSN 1070-9622/13/$27.50

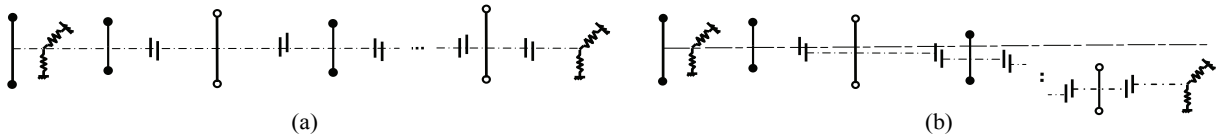

Fig. 1. Schematic diagrams of a misaligned rotor with (a) local offset, and (b) global offset; •: unbalanced mass, ‖: coupler.

was usually no differentiation between local and global coupler offset. The authors intend to model and discuss these differences in this article. The local coupler misalignment can be treated as an eccentricity between coupler's two disks as Fig. 1(a) shows. The global offset is yet shown in Fig. 1(b). The difference between them is the shaft's center line well aligned with the front shaft after local offset but deviated a distance after global offset. The followings are some researches on coupler misalignment/offset Dewell and Mitchell [13] experimentally studied parallel (offset) and angular misalignment of a metallic-disk-type coupling. They used real time analyzer and found out n$\times$ frequencies appeared in the response due to misalignment. They further suggested 2$\times$ and 4$\times$ components be used for misalignment diagnosis. They however suggested no method to distinguish the parallel and angular misalignment over any harmonic. Xu and Marangoni used a universal joint to model misalignment and utilized the component mode synthesis to analytically [14] study and experimentally [15] validate their calculations. In their model, the misalignment effect was represented by an additional bending moment of even multiples of rotational speed. Although they included multiple frequencies in numerical calculations but only showed the 2$\times$ component response and suggested unbalance and misalignment could be characterized by 1$\times$ and 2$\times$ component, respectively. Sekhar and Prabhu [16] used higher order finite element to study both parallel (0 to 2.03 mm) and angular misalignment (0 to 0.6 deg) of a rotor-bearing system. In their model, they used three bending moments and three axial forces of different values to model the parallel and angular misalignment and obtained similar conclusions as [14]. They also concluded that the misalignment had little effect on rotor's critical speeds. Lee and Lee [17] employed FEM to solve for angular, parallel, and combined misaligned rotor-bearing system. The influences were shown extensively through whirling orbits. In that paper, they concluded the whirling orbits tended not to change for parallel misalignment. Al-Hussain and Redmond [18] analytically derived the equations of two Jeffcott rotors with rigid coupling in parallel misalignment. In their results, there appeared just 1$\times$ component unlike the others who obtained n$\times$ instead. Al-Hussain [19] further extended his previous work to the stability analysis. Saavedra and Ramirz [20] proposed a theoretical model of a rotor-bearing system using a new coupling finite element stiffness matrix and discussed the vibration behaviour due to shaft misalignment and residual unbalance. Their results showed the vibration induced by shaft misalignment was due to the variation in coupling stiffness and the generated forcing frequencies were harmonics of the rotational speed. Experimental results [21] were presented to validate the theoretical model. Huang [22] analyzed torsional vibration characteristics of a shaft with parallel misalignment and indicated that the misalignment excited the tosional vibration at 1$\times$ rotating frequency. Hili et al. [23] presented a theoretical model to analyse parallel and angular misalignment from vibration response, and proposed to diagnose the shaft misalignment from the harmonics of running speed. Lees [24] investigated the characteristic of misalignment in rigidly coupled rotors mounted on idealised linear bearing. The vibration response at twice the synchronous speed due to existence of misalignment was evaluated. Lately et al. [25,26] used Timoshenko beam elements in FEM to investigated parallel and angular misalignment. They experimentally measured misalignment-induced forces and used them as excitation nodal forces in the finite element model. Their results showed 1$\times$ predominated in all vibrations, axial, torsional, and lateral. The higher harmonics although showed as well but were much weaker than 1$\times$ component. Most importantly, the authors discovered the backward frequencies, i.e., $-$n$\times$, accompanied with misalignment and suggested use them for misalignment diagnosis.

The authors once developed the transfer matrix for a coupler offset and in conjunction with other elements to form a TMM for rotors. In that paper, the mass effect of coupler's disks was yet neglected. In the present study, the authors include not only the coupler's mass effect but also illustrate two different types of offset as shown in Fig. 1. In Fig. 1(a), the coupler offset occurs only at coupler's disks and all the shaft axes are well aligned with the rotating axis. The authors call it local offset. As to Fig. 1(b), each shaft section behind a coupler is parallelly shifted by an amount e such that all the shafts misaligned afterwards. It is here called global offset. The authors here derive rotor dynamics due to local and global offset in a TMM. It is expected global offset should impose more significant

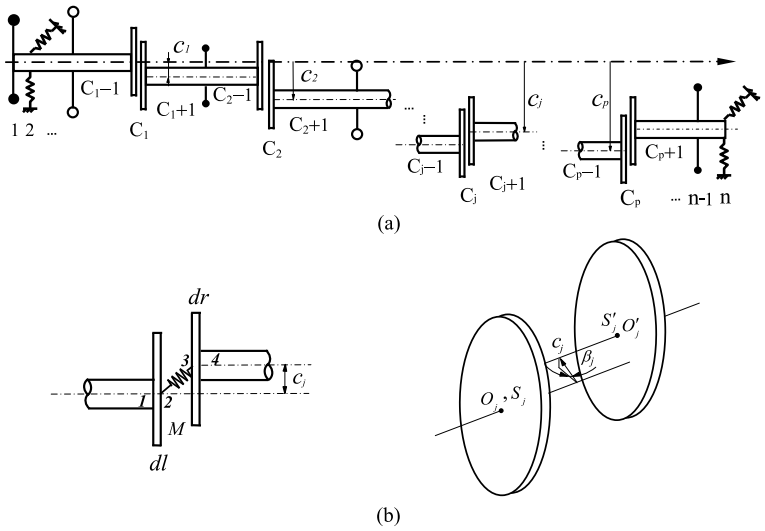

Fig. 2. Schematic diagrams of a misaligned rotor for (a) the global offset, and (b) the configuration of offset.

dynamic effects than local offset since all the offsets accumulate one after the others. In the derivation, a TMM for rotor systems containing multiple offsets is formed and the dynamic effects are looked into. Numerical examples of local and global offset for a typical rotor system are then studied and compared with.

2. Transfer matrices for global and local offset

A rotor system contains commonly seen elements, such as flexible shafts, disks, bearing supports and shafts offset are shown schematically in Fig. 2(a). Transfer matrices of unbalanced disks, bearings, rotating shafts, etc., though they might differ in some respects, are frequently seen and can be referred to the existing literature, e.g., reference [12,27]. The present derivation focuses on the TM of global and local offset and looks into their effects.

Consider a coupler composed of two disks and in between there exists a rigid or elastic restraint as shown in Fig. 2(b). The elastic restraint is represented by one radial and one bending linear spring. The left and right disks of a typical coupler are denoted *dl* and *dr*, respectively.

First of all, the transfer relation of coupler's left disk, i.e., from point 1 to point 2 can be written as

$$\{S\}_{dl}^{R} = [T_{dl}]\,\{S\}_{dl}^{L} \tag{1}$$

where$\{S\}_{dl}$ and $[T_{dl}]$ are the state vector and the transfer matrix of the left disk, respectively. Furthermore, the transfer relation between left and right side of such an offset (from point 2 to point 3) have been derived by the authors in reference [12] as the follow

$$\{S\}_{M}^{R} = [T_M]\,\{S\}_{M}^{L} + \{c\} \tag{2}$$

where $[T_M]$ is the transfer matrix for the elastic restraint between two disks, and $\{c\}$ is the offset vector,

$$\{c\}_{17\times 1} = \left\{ c\sin\beta\ 0\ 0\ 0\ c\sin\beta\ 0\ 0\ 0\ c\cos\beta\ 0\ 0\ 0\ -c\cos\beta\ 0\ 0\ 0\ 0\ 0\ 0 \right\}^{T} \tag{3}$$

where c is the shaft's offset distance and β is the phase angle as shown in Fig. 2(b). Since $\{S\}_{M}^{L} = \{S\}_{dl}^{R}$, with the help of Eq. (2), the transfer relation from point 1 to point 3 can be combined as

$$\{S\}_{M}^{R} = [T_M][T_{dl}]\,\{S\}_{dl}^{L} + \{c\} \tag{4}$$

Similarly, the TM from point 1 to point 4 can be derived to be

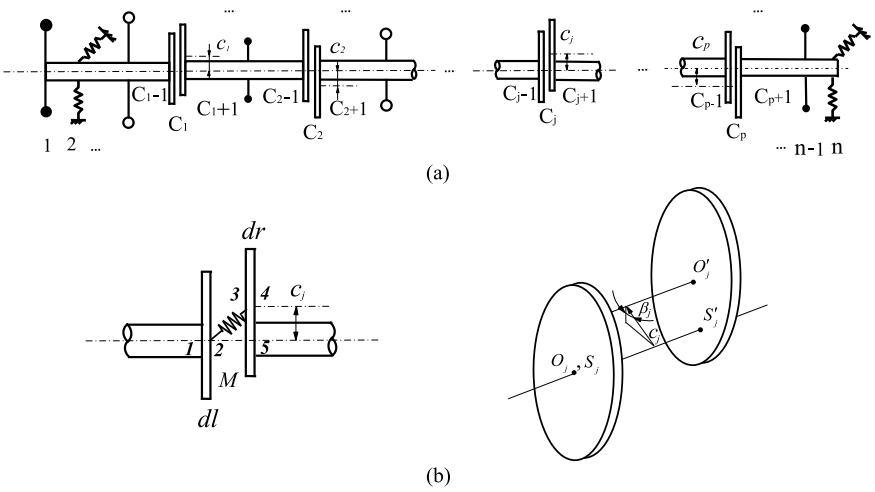

Fig. 3. Schematic diagrams of a misaligned rotor for (a) the local offset, and (b) the configuration of offset.

$$\begin{aligned}\{S\}_{dr}^{R} &= [T_{dr}]\{S\}_{dr}^{L}, \text{where } \{S\}_{dr}^{L} = \{S\}_{M}^{R} \\ &= [T_{dr}]\left([T_M][T_{dl}]\{S\}_{dl}^{L} + \{c\}\right) \\ &= [T_{dr}][T_M][T_{dl}]\{S\}_{dl}^{L} + [T_{dr}]\{c\}\end{aligned} \tag{5}$$

where $[T_{dr}]$ is the transfer matrix of right disk, or in a short form,

$$\{S\}_{C}^{R} = [T_C]\{S\}_{C}^{L} + \{e_g\} \tag{6}$$

where $[T_C] = [T_{dr}][T_M][T_{dl}]$, called the coupler TM, and $\{e_g\}$ is called the global offset vector,

$$\{e_g\} = \left\{\{e_g\}_a \{e_g\}_b 0\right\}^T \tag{7a}$$

where

$$\begin{cases}\{e_g\}_a = \left\{c\sin\beta\ 0\ 0\ -m\omega^2\cdot c\cos\beta\ c\sin\beta\ 0\ 0\ -m\omega^2\cdot c\sin\beta\right\}^T \\ \{e_g\}_b = \left\{c\cos\beta\ 0\ 0\ -m\omega^2\cdot c\cos\beta\ -c\cos\beta\ 0\ 0\ m\omega^2\cdot c\sin\beta\right\}^T\end{cases} \tag{7b}$$

Figure 3 shows a similar but different offset, in which only are the coupler disks displaced not the shafts. By the same derivation, the state vector from point 1 to point 5 can be expressed as

$$\begin{aligned}\{S\}_{dr}^{R} &= [T_{dr}][T_M][T_{dl}]\{S\}_{dl}^{L} + [T_{dr}]\{c\} - \{c\} \\ &= [T_{dr}][T_M][T_{dl}]\{S\}_{dl}^{L} + ([T_{dr}] - [I])\{c\}\end{aligned} \tag{8}$$

or in short,

$$\{S\}_{C}^{R} = [T_C]\{S\}_{C}^{L} + \{e_l\} \tag{9}$$

where $\{e_l\}$ is called the local offset vector,

$$\{e_l\} = \left\{\{e_l\}_a \{e_l\}_b 0\right\}^T \tag{10a}$$

where

$$\begin{cases}\{e_l\}_a = \left\{0\ 0\ 0\ -m\omega^2\cdot c\sin\beta\ 0\ 0\ 0\ -m\omega^2\cdot c\sin\beta\right\}^T \\ \{e_l\}_b = \left\{0\ 0\ 0\ -m\omega^2\cdot c\cos\beta\ 0\ 0\ 0\ m\omega^2\cdot c\cos\beta\right\}^T\end{cases} \tag{10b}$$

Equations (6) and (9) are the transfer equations of the global and local offset, respectively. $[T_C]$, similar to the other elements, is the transfer matrix that links the left and right state of the coupler, yet $\{e_g\}$ and $\{e_l\}$, the offset

vectors, play as exciting forces. It will be seen after multiplication to the couplers right matrices, all components to the right of the offset contribution to the excitation. That means the driven parts behind the offset acts as a whole excitation to the rotor.

Additionally, by comparing Eqs (7) and (10), the difference between the global offset and local offset is depicted below. For the global offset, the exciting source is mainly resulted from the shaft's offset. As to the local offset, since its vector only has shear force, the magnitude of the exciting force is the centrifugal force of the eccentric disk rotating about the shaft axis, i.e., the local offset are caused by the unbalance force generated by the coupler's offset. However, their subsequent effect was a combined displacement excitation behind the coupler.

3. Total transfer matrix and response analysis

In Figs 2(a) and 3(a), each element (field) from left to right is assigned a number. Let the first coupler be numbered C_1 and its left and right adjacent elements are numbered $C_1 - 1$ and $C_1 + 1$, respectively. c_j denotes the offset (global or local) of the j^{th} coupler, element numer C_j. With the derived offset TM and in conjunction with the other elements TM, the overall transfer matrix for the system containing p offsets is hence evolved to be

$$\{S\}_n^R = \prod_{i=n}^{1}[T]_i \{S\}_1^L + \underline{\prod_{i=n}^{C_1+1}[T]_i\{e\}_1 + \cdots + \prod_{i=n}^{C_j+1}[T]_i\{e\}_j + \cdots + \prod_{i=n}^{C_p+1}[T]_i\{e\}_p} \tag{11}$$

or, more simply

$$\begin{aligned}\{S\}_n^R &= [T^u]\{S\}_1^L + \underline{[T^{C_1+1}]\{e\}_1 + \cdots + [T^{C_j+1}]\{e\}_j + \cdots + [T^{C_p+1}]\{e\}_p} \\ &= [T^u]\{S\}_1^L + \underline{\sum_{j=1}^{p}[T^{C_j+1}]\{e\}_j}\end{aligned} \tag{12}$$

where $[T]_i$ denotes the i^{th} element transfer matrix, it can be a shaft, disk, or bearing, etc. $\{S\}_1^L$ represents the left state of unit 1, $\{S\}_n^R$ is the right state of unit n. $[T^u]$ is the so-called overall transfer matrix yielded by consecutive multiplications of all elements transfer matrices. $[T^{C_j+1}]$ is the multiplications of the transfer matrices to the right of C_j^{th} offset, i.e., from $C_j + 1$ to n. $\{e\}_j$ denotes the offset vector of the j^{th} coupler, it can be global offset vector $\{e_g\}$ or local offset vector $\{e_l\}$. Note that in the above equations, those terms underlined are offset-induced transfer matrices.

Equation (12), to the authors knowledge, is for the first time ever derived the TMM for rotors with multi-offset global and local offset. Substituting the appropriate boundary conditions into Eq. (12), a 8×1 equation yields

$$[T^u]' \times \{S'\}^L = -\{u\} - \sum_{j=1}^{p}[T^{C_j+1}]' \cdot \{e\}_j' \tag{13}$$

with the condensed offset vector $\{e'\}_j = [T_{dr}]\{c_j'\}$ or $\{e'\}_j = ([T_{dr}] - [I])\{c_j'\}$, and

$$\{c_j'\}_{4\times1} = \{-c_j \sin\beta_j, -c_j \sin\beta_j, -c_j \cos\beta_j, c_j \cos\beta_j\}^T \tag{14}$$

where $[T^u]', \{u\}$are the degenerated matrices of $[T^u]$, $[T^{C_j+1}]'$ is the degenerated matrices from $[T^{C_j+1}]$, i.e., by picking up corresponding rows and columns from $[T^u]$ and $[T^{C_j+1}]$ according to left and right boundaries. $\{S'\}$ and $\{c'\}$ are the degenerated matrices of $\{S\}$ and $\{c\}$, respectively. The rows (right boundary) and columns (left boundary) to be picked up based upon different boundary conditions are summarized in Table 1 Note that the offset vectors $\{e_j\}$, $\{e_j'\}$denoted above can be global or local deponding on the coupler's situation.

Equation (13) contains rotor response due to two sources, the first term on the right-hand side is the commonly seen disk's unbalanced excitation, and the second term is newly derived offset excitation. The offset appears to be a much more complicated excitation mechanism since all the elements behind offset participate in the excitation. Provided no offset ($c_j = 0, j = 1, p$), $\{c_j\} = \{0\}$, and Eq. (13), yields an unbalanced response analysis as derived by many others [3,4,6,14].

Table 1
Entries of $[T^u]'$, $\{S'\}$, $\{u\}$ and $[T^{C_j+1}]'$

Left b.c	Columns of $[T^u]'$, $\{S'\}$ from $[T^u]$ and $\{S\}$	Right b.c	Rows of $[T^u]'$
Free	1,2,5,6,9,10,13,14	Free	3,4,7,8,11,12,15,16
Simple	2,4,6,8,10,12,14,16	Simple	1,3,5,7,9,11,13,15
Clamped	3,4,7,8,11,12,15,16	Clamped	1,2,5,6,9,10,13,14
Sliding	1,3,5,7,9,11,13,15	Sliding	2,4,6,8,10,12,14,16
Left b.c	Columns of $\{u\}$ from $[T^u]$ (unbalance)	Right b.c	Rows of $\{u\}$
Free	17	Free	3,4,7,8,11,12,15,16
Simple	17	Simple	1,3,5,7,9,11,13,15
Clamped	17	Clamped	1,2,5,6,9,10,13,14
Sliding	17	Sliding	2,4,6,8,10,12,14,16
Left b.c	Columns of $[T^{C_j+1}]'$ from $[T^{C_j+1}]$ (offset)	Right b.c	Rows of $[T^{C_j+1}]'$
Free	1,5,9,13	Free	3,4,7,8,11,12,15,16
Simple	1,5,9,13	Simple	1,3,5,7,9,11,13,15
Clamped	1,5,9,13	Clamped	1,2,5,6,9,10,13,14
Sliding	1,5,9,13	Sliding	2,4,6,8,10,12,14,16

Table 2
Material and geometric parameters of illustrated example

Disk No.	Mass (kg)	Polar inertia ($kg.m^2 \times 10^{-2}$)	Diameteral inertia ($kg.m^2 \times 10^{-2}$)
1	11.38	19.53	9.82
5	7.88	16.7	8.35
7	7.7	17.61	8.8
14	7.7	17.61	8.8
18	21.7	44.48	22.24
Shaft No.	Length (cm)	Radius (cm)	
2	8.89		
4	1.6		
6	9.68	Outer Radius = 2.950 cm	
8	7.52		
10	25	Inner Radius = 1.680 cm	
12	20		
13	15		
15	20		
17	12.45		
19	7.8		

4. Numerical results

In the following, examples demonstrating the influence of local and global offset via the developed TMM are illustrated. The rotor system shown in Fig. 4, where configuration and material of the system are similar to Ref. [28], consists of five bearings, five rigid disks, two unbalanced, and one tenstage flexible shaft. The Young's modulus is $E = 20.69 \times 10^{10}\ N/m^2$, density $\rho = 8193.0\ kg/m^3$ and the five bearings are assumed, though not necessarily, the same ($K_{yy} = 2.850 \times 10^7\ N/m, K_{zz} = 1.000 \times 10^7\ N/m, K_{\phi\phi} = 4150\ N \cdot m/rad, K_{\theta\theta} = 1520\ N \cdot m/rad$). Detailed dimensions of disks and shafts are given in Table 2.

In general, the inertia of coupler's disks are neglected [12,16]. To realize the influence of coupler's disks' effect, Fig. 5 shows the responses with and without coupler's inertia considered, where mass $= 0.813\ kg$, polar mass moment of inertia $= 5.867 \times 10^{-4}\ kg\text{-}m^2$ and diametral mass moment of inertia $= 3.357 \times 10^{-4}\ kg\text{-}m^2$. It is seen the inertia pull the critical speeds down noticeably, 0.248%, 2.06% and 0.422%, particularly the second one. From the results, the authors feel more comfortable to include the coupler's disks.

It is assumed one local/global offset at stations A, B as shown in Figs 4(a) and 4(b), respectively. Equations (12) and (14) are viable for multi-offset of local and global, but here we will consider only one offset of $c = 1.0 \times 10^3\ m$. To begin with, we first look into the influences of coupler linear stiffness on rotor's forward critical speeds. Figure 6 shows the first three critical speeds as functions of the coupler linear stiffness K_L. It is seen as K_L falls in the

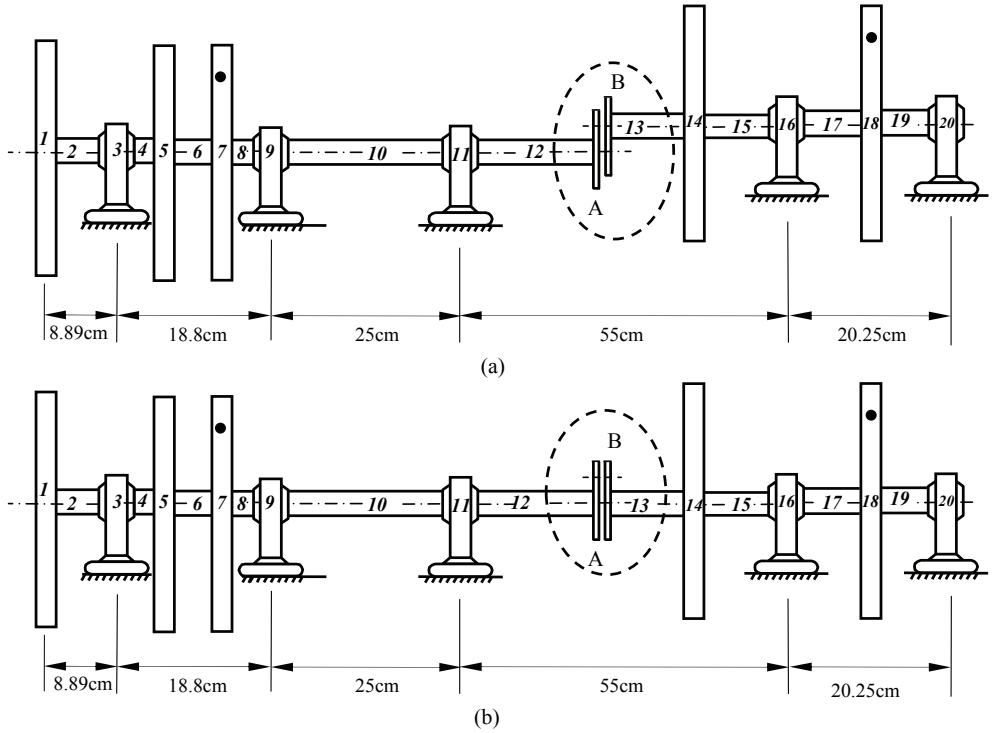

Fig. 4. Example of a misaligned rotor (a) global offset, and (b) local offset, ●: unbalanced mass.

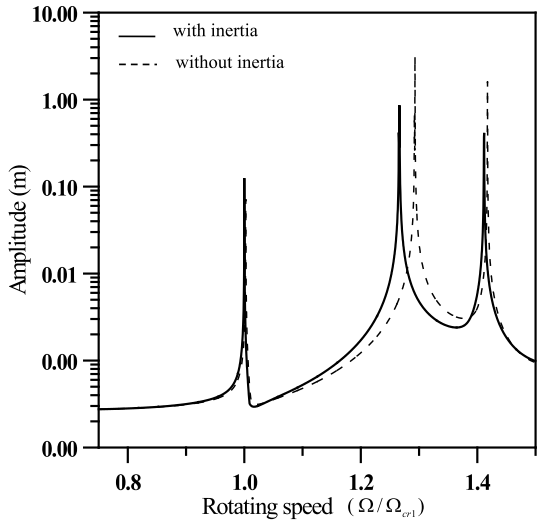

Fig. 5. Critical speed of rotor with and without coupler's inertia.

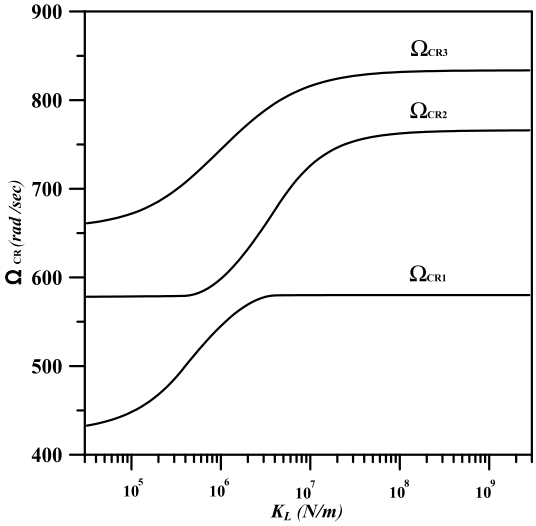

Fig. 6. Influence of coupler linear stiffness on critical speeds.

region of $0.75(10^5)$ N-$m \sim 1.2(10^7)$ N-m (sensitive area), the critical speeds are very sensitive to K_L such that a slight change results in significant change in critical speeds. When K_L is either below the 0.75×10^6 N-m or over 0.12×10^8 N-m the critical speeds barely change. In following examples, the coupler linear stiffness is chosen in the sensitive area, unless otherwise specified. Next, the first three modes without offset (dashed), with global offset and local offset are illustrated in Fig. 7. It is seen the modes basically retain the original shapes but appear different jumps at the offset.

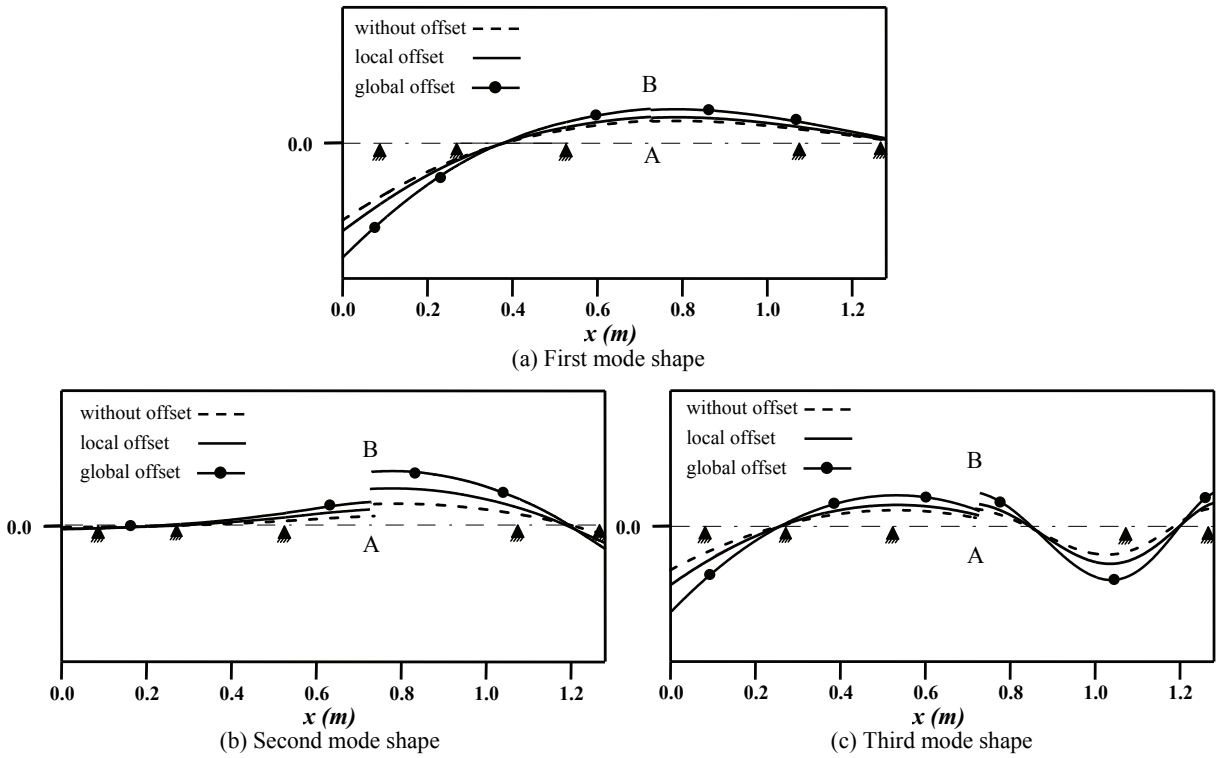

Fig. 7. First three mode shapes for local and global offset.

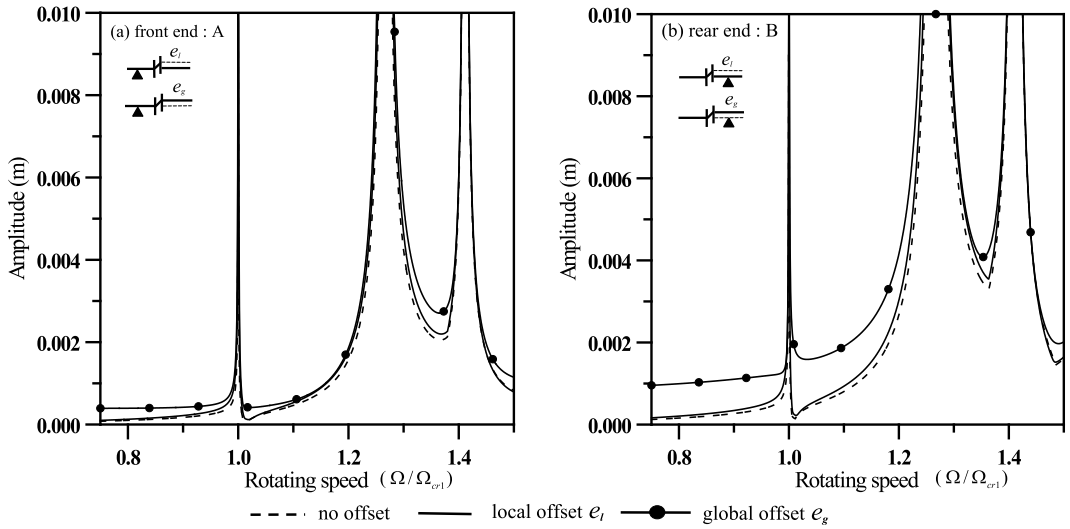

Fig. 8. FRF due to disk imbalance and offset (a) at station 12, and (b) at station 13.

Figure 8 shows the FRF of the rotor at 12^{th} and 13^{th} stations for local/global offset. The FRF of no offset, simply due to unbalance, is overlapped as dash curves for comparison. It is first noticed FRF's show no extra peaks, this agrees with other researcher's conclusion that offset does not change the critical speeds [16].

From Fig. 8(a) it is seen the response in front of the local offset (A) is barely changed so that its FRF almost coincides with that of no offset. The difference is yet more obvious in the global offset. The effect of global offset

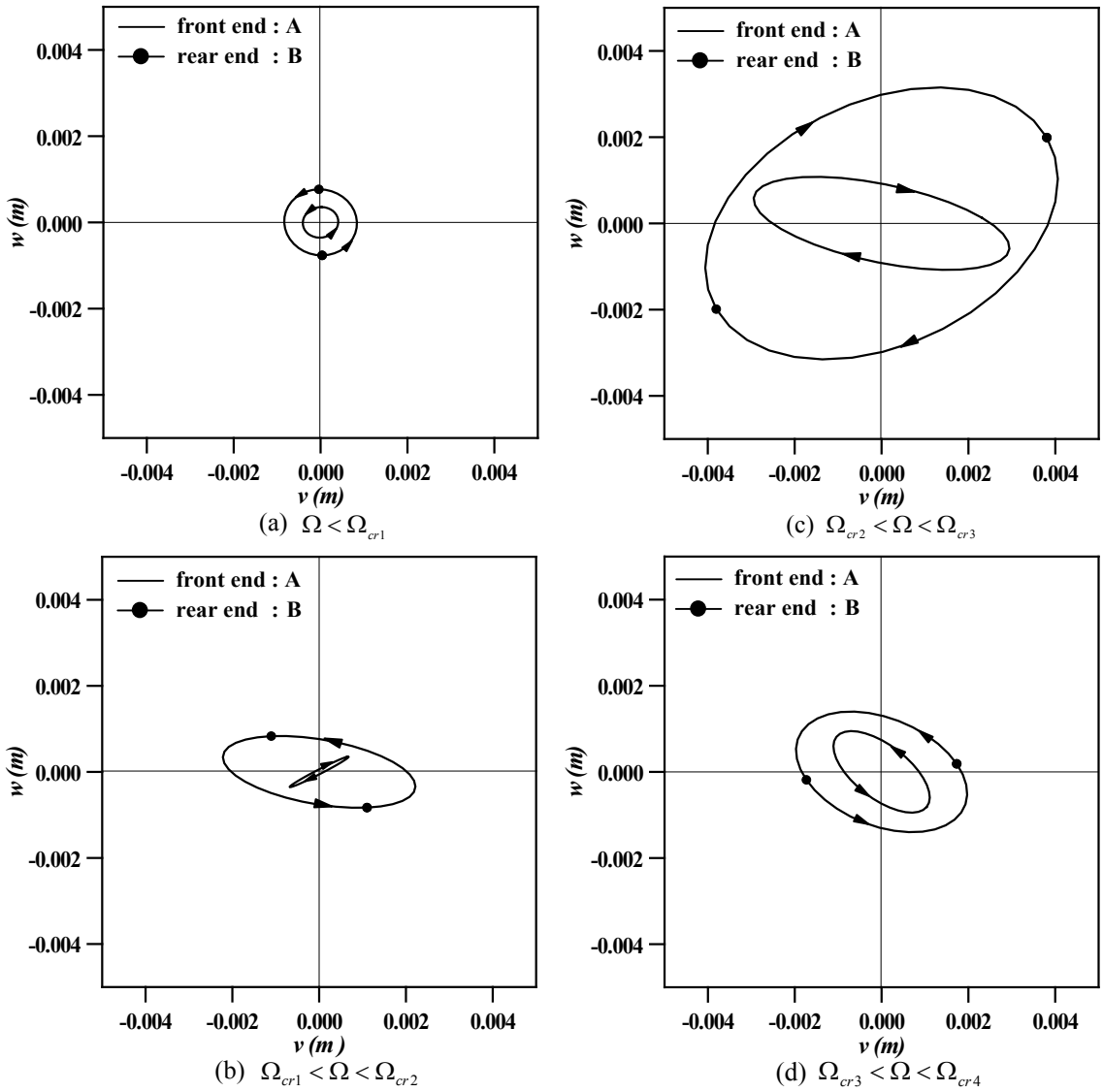

Fig. 9. Whirling orbits of global offset for different rotational speed.

becomes more significant as the rotaion exceeds the first critical speed. As to the FRF's behind the offset, Fig. 8(b), their effects appear to be significant for both local and global offset. Similary, the global offset invokes larger response than the local one.

The whirling orbits under different rotational speeds are illustrated as well. The 12^{th} (A) and 13^{th} (B), corresponding to the front and the rear end of the coupler, are drawn for their orbits. The global and local offset cases are shown in Figs 9 and 10, respectively. Four plots corresponding to (a) $\Omega < \Omega_{cr1}$, (b) $\Omega_{cr1} < \Omega < \Omega_{cr2}$, (c) $\Omega_{cr2} < \Omega < \Omega_{cr3}$, and (d) $\Omega_{cr3} < \Omega < \Omega_{cr4}$ are shown. One can observe that the whirling orbit varies with the rotational speeds as expected. From Fig. 9, it is seen when the rotational speed varies from $\Omega < \Omega_{cr1}$ to $\Omega_{cr1} < \Omega < \Omega_{cr2}$, the orbit of driving (A) switches from forward whirl to backward whirl but driven (B) remains forward whirl, as shown in Figs 9(a) and 9(b). At the rotational speed of $\Omega_{cr2} < \Omega < \Omega_{cr3}$, driven (B) end also switches from forward whirl to backward whirl as shown in Fig. 9(c). However, when the rotational speed $\Omega_{cr3} < \Omega < \Omega_{cr4}$, the orbits switch from backward whirl to forward whirl again as shown in Fig. 9(d). A similar behaviour is also observed for local offset except driving (A) and driven (B) remains forward whirl at the rotational

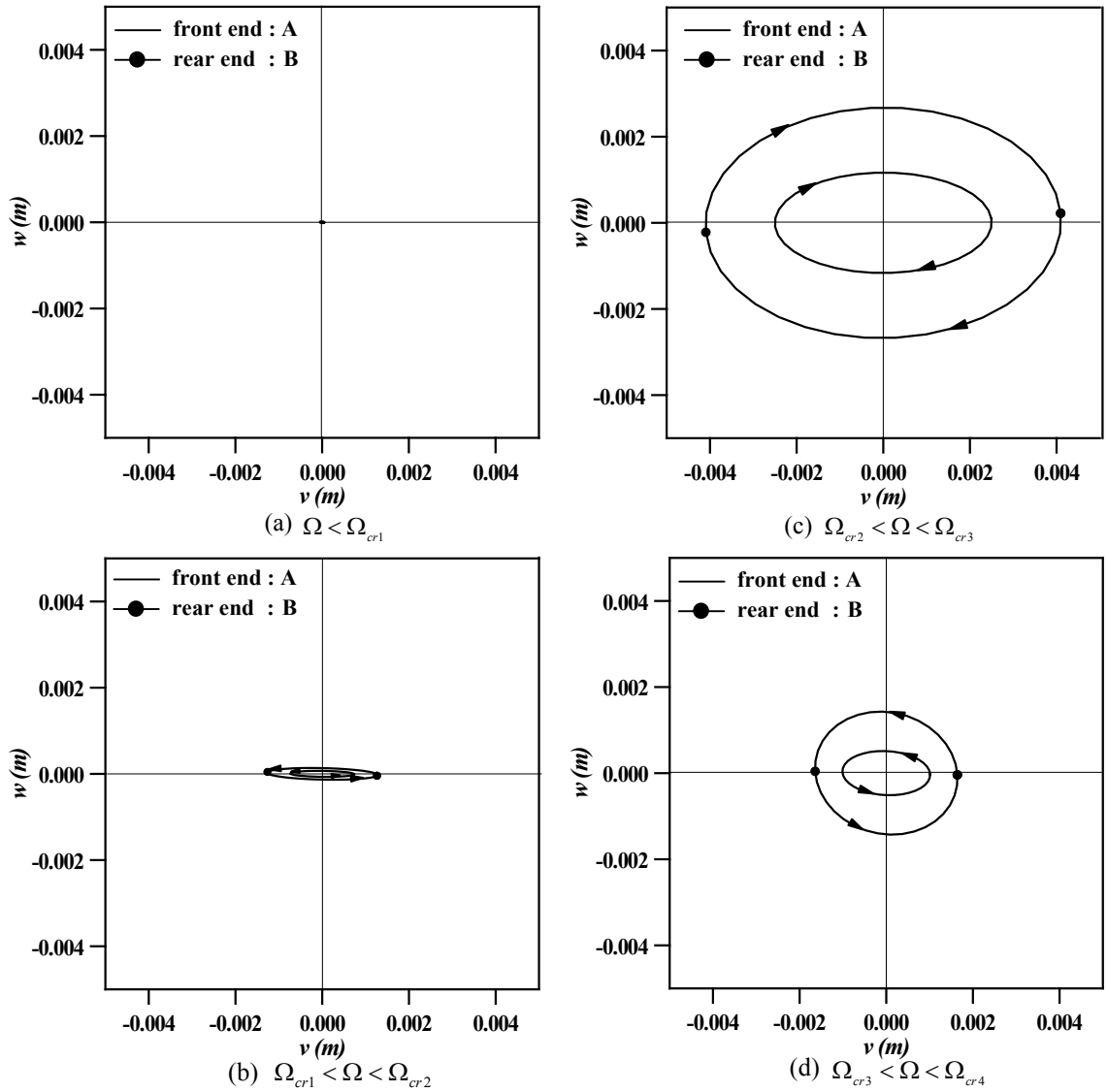

Fig. 10. Whirling orbits of local offset for different rotational speed.

speed of $\Omega_{cr1} < \Omega < \Omega_{cr2}$, as shown in Fig. 10(b). Whirling orbits are a relatively complicated phenomenon and it frequently happens that once rotation exceeds some critical speeds; the whirl changes its orientation, i.e., from forward to backward or vice versa. It may be noted that the whirl orbit varies with different locations along its axis even though it is at the same rotational speed. Figures 9 and 10 also reveal that global offset induces much larger orbit radii than the local one at both front and rear ends of the coupler.

5. Discussion and conclusions

The authors derived the transfer matrix of a rotor with global and local offset and obtained a general TMM. Two types of offset, global and local, on the rotor dynamic behaviour were demonstrated and investigated via showing the vibration modes, whirling orbit plots and FRF's. By inspecting Eq. (12) it is seen both global and local offsets add additional terms to the equation's right side. It implies the offset plays as an extra excitation similar to imbalance

force. Also because the offset does not enter the overall transfer matrix, it can be concluded that the offset does not change the rotor's critical speeds, similar to the conclusion of [16]. The comparisons of global and local offset showed global offset induces much larger response amplitude at both front and rear end of a coupler. As rotational speed falls within the third and fourth critical speed, the orbits switch direction and this phenomenon is not changed by offset, either global or local offset.

TMM derivation and numerical results in the present studies revealed that offset induced the rotor's lateral response at the same frequency as rotational speed ($1\times$) and that was unlike most of the other researches where multiple integer ($n\times$) components were found. Though reference [18] obtained similar results to the present's and authors of that paper attributed the absence of $2\times$ components to the no consideration of non-linear effects of bearing and asymmetries of shafts. We, however, believe that the reason of $n\times$ components not showing in our derivation is due to the fact that the coupler's torsional vibration was not considered. Since the coupler will transmit torque in addition to lateral vibration and as long as the torsional flexibility of the coupler is taken into account, the driven shaft will fluctuate in torsion so that it causes a fluctuation of rotation. The fluctuation of rotational speed will consequently generate cyclic forces and moments effects on lateral vibration. The cyclic forces in general will result in excitation of $n\times$ components as described in [14–16].

Acknowledgments

The support for this research by the National Science Council, NSC 95-2221-E-011-010, is gratefully acknowledged.

References

[1] H.D. Nelson and J.M. McVeigh, The dynamics of rotor-bearing systems using finite elements, *ASME Journal of Engineering for Industry* **98**(2) (1976), 593–600.
[2] H.N. Özgüven, On the critical speed of continuous shaft-disk systems, *ASME Journal of Vibration, Acoustics, Stress and Reliability in Design* **106** (1) (1984), 59–61.
[3] H.N. Özgüven and Z.L. Özkan, Whirl speeds and unbalance response of multi-bearing rotors using finite elements, *ASME Journal of Vibration, Acoustics, Stress and Reliability in Design* **106** (1) (1984), 72–79.
[4] J. Gu, An improved transfer matrix-direct integration method for rotor dynamics, *ASME Journal of Vibration, Acoustics, Stress and Reliability in Design* **108** (2) (1986), 182–188.
[5] M.A. Prohl, A general method for critical speeds of flexible rotors, *Journal of Applied Mechanics* **67** (1945), A142–A148.
[6] J.W. Lund and F.K. Orcutt, Calculations and experiments on the unbalance response of a flexible rotor, *ASME Journal of Engineering for Industry* **89** (4) (1967), 785–796.
[7] J.W. Lund, Stability and damped critical speeds of a flexible rotor in fluid-film bearings, *ASME Journal of Engineering for Industry* **96** (2) (1974), 509–517.
[8] S.W. Chao and S.C. Huang, On the flexural vibrations of shaft-disk systems using a modified transfer matrix method, *Proceedings of the 6^{th} National Conference of the CSME*, Taiwan, ROC, 1989, pp. 1607–1618.
[9] N.F. Rieger and S. Zhou, Development and verification of transfer matrix unbalance response procedure for three-level rotor-foundation systems, *ASME Journal of Vibration and Acoustics* **20** (1) (1998), 240–251.
[10] J.W. Zu and Z. Ji, An improved transfer matrix method for steady-state analysis of nonlinear rotor-bearing systems, *ASME Journal of Engineering for Gas Turbines and Power* **124**(2) (2002), 303–310.
[11] B.B. Maharathi, P.R. Dash and A.K. Behera, Dynamic behavior analysis of a dual-rotor system using the transfer matrix method, *International Journal of Acoustics and Vibrations* **9**(3) (2004), 115–128.
[12] C.Y. Tsai and S.C. Huang, Transfer matrix for rotor coupler with parallel misalignment, *Journal of Mechanical Science and Technology* **23**(5) (2009), 1383–1395.
[13] D.L. Dewell and L.D. Mitchell, Detection of a misaligned disk coupling using spectrum analysis, *ASME Journal of Vibration, Acoustics, Stress and Reliability in Design* **106**(1) (1984), 9–16.
[14] M. Xu and R.D. Marangoni, Vibration analysis of a motor-flexible coupling-rotor system subject to misalignment and unbalance, Part I: Theoretical model and analysis, *Journal of Sound and Vibration* **176**(5) (1994), 663–679.
[15] M. Xu and R.D. Marangoni, Vibration analysis of a motor-flexible coupling-rotor system subject to misalignment and unbalance, Part II: Experimental validation, *Journal of Sound and Vibration* **176** (5) (1994), 681–691.
[16] A.S. Sekhar and B.S. Prabhu, Effects of coupling misalignment on vibrations of rotating machinery, *Journal of Sound and Vibration* **185**(4) (1995), 655–671.
[17] Y.S. Lee and C.W. Lee, Modelling and vibration analysis of misaligned rotor-ball bearing systems, *Journal of Sound and Vibration* **224**(1) (1999), 17–32.

[18] K.M. Al-Hussain and I. Redmond, Dynamic response of two rotors connected by rigid mechanical coupling with parallel misalignment, *Journal of Sound and Vibration* **249**(3) (2002), 483–498.
[19] K.M. Al-Hussain, Dynamic stability of two rigid rotors connected by a flexible coupling with angular misalignment, *Journal of Sound and Vibration*, **266** (2) (2003), 217–234.
[20] P.N. Saavedra and D.E. Ramirez, Vibration analysis of rotors for identification of shaft misalignment, Part 1: Theoretical analysis, *Proceedings of the Institution of Mechanical Engineers, Part C: Journal of Mechanical Engineering Science* **218**(9) (2004), 971–985.
[21] P.N. Saavedra and D.E. Ramirez, Vibration analysis of rotors for the identification of shaft misalignment, Part 2: Experimental validation, *Proceedings of the Institution of Mechanical Engineers, Part C: Journal of Mechanical Engineering Science* **218**(9) (2004), 987–999.
[22] D. Huang, Characteristics of torsional vibrations of a shaft system with parallel misalignment, *Proceedings of the Institution of Mechanical Engineers, Part C: Journal of Mechanical Engineering Science* **219** (11) (2005), 1219–1224.
[23] M.A. Hili, T. Fakhfakh, L. Hammami and M. Haddar, Shaft misalignment effect on bearings dynamical behavior, *International Journal of Advanced Manufacturing Technology* **26** (2005), 615–622.
[24] A.W. Lees, Misalignment in rigidly coupled rotors, *Journal of Sound and Vibration* **305** (2007), 261–271.
[25] T.H. Patel and A.K. Darpe, Vibration Response of Misaligned Rotors, *Journal of Sound and Vibration* **325** (2009), 609–628.
[26] T.H. Patel and A.K. Darpe, Experimental investigations on vibration response of misaligned rotors, *Mechanical Systems and Signal Processing* **23** (2009), 2236–2252.
[27] J.S. Rao, Rotor dynamics, Wiley Eastern Limited, 1983.
[28] M. Rajan, S.D. Rajan, H.D. Nelson and W.J. Chen, Optimal placement of critical peeds in rotor-bearing systems, *ASME Journal of Vibration, Acoustics, Stress and Reliability in Design* **109** (1987), 152–157.